Control of peptide nanotube diameter by chemical modifications of an aromatic residue involved in a single close contact

Christophe Tarabout[a,1], Stéphane Roux[a,b,1], Frédéric Gobeaux[c,d,1], Nicolas Fay[c,d,1], Emilie Pouget[a], Cristelle Meriadec[a], Melinda Ligeti[b], Daniel Thomas[e], Maarten IJsselstijn[b], François Besselievre[b], David-Alexandre Buisson[b], Jean-Marc Verbavatz[c,d], Michel Petitjean[c,d], Céline Valéry[f], Lionel Perrin[c,d], Bernard Rousseau[b], Franck Artzner[a,2], Maité Paternostre[c,d,2], and Jean-Christophe Cintrat[b,2]

[a]Unité Mixte de Recherche 6251, Centre National de la Recherche Scientifique and Université Rennes 1, F-35 Rennes, France; [b]Institut de Biologie et de Technologies de Saclay/Service de Chimie Bioorganique et Marquage, Commissariat à l'Énergie Atomique et aux Energies Alternatives-Saclay, F-91191 Gif-sur-Yvette, France; [c]Institut de Biologie et de Technologies de Saclay/Service de Bioénergétique, Biologie Structurale et Mécanismes, Commissariat à l'Énergie Atomique et aux Énergies Alternatives-Saclay, F-91191 Gif-sur-Yvette, France; [d]Unité de Recherche Associée 2096, Centre Nationale de la Recherche Scientifique, Commissariat à l'Énergie Atomique et aux Energies Alternatives-Saclay, F-91191 Gif-sur-Yvette, France; [e]Unité Mixte de Recherche 6026, Centre National de la Recherche Scientifique and Université Rennes 1, F-35042 Rennes Cedex, France; and [f]Ipsen-Pharma, san Feliu de Llobregat, Barcelona, Spain

Edited by Chad A. Mirkin, Northwestern University, Evanston, IL, and approved March 21, 2011 (received for review November 18, 2010)

Supramolecular self-assembly is an attractive pathway for bottom-up synthesis of novel nanomaterials. In particular, this approach allows the spontaneous formation of structures of well-defined shapes and monodisperse characteristic sizes. Because nanotechnology mainly relies on size-dependent physical phenomena, the control of monodispersity is required, but the possibility of tuning the size is also essential. For self-assembling systems, shape, size, and monodispersity are mainly settled by the chemical structure of the building block. Attempts to change the size notably by chemical modification usually end up with the loss of self-assembly. Here, we generated a library of 17 peptides forming nanotubes of monodisperse diameter ranging from 10 to 36 nm. A structural model taking into account close contacts explains how a modification of a few Å of a single aromatic residue induces a fourfold increase in nanotube diameter. The application of such a strategy is demonstrated by the formation of silica nanotubes of various diameters.

size control | mineralization | structural approach | size prediction

Many fundamental properties of materials are characterized by length scales on the order of 10 to 200 Å. If a crystal is made such that at least one of its dimensions is smaller than the length scale of some property, then that property is "confined" and becomes dependent on the size and shape of what is now called a "quantum crystal." This is true, for example, of electron conduction, but also for the optical and other physical and chemical (e.g., oxidation-reduction) properties of semiconductor nanoparticles that become sensitive to their size and shape. Among the most spectacular and well-known examples are the so called quantum dots, the optical properties of which being directly linked to their size (1). There has been rapid progress in the development of nanomaterials such as nanowires, nanotubes, nanoparticles, and nanocrystals, which show superior electronic, magnetic, optical, and mechanical properties as compared with their bulk counterparts. These materials are extremely attractive as building blocks for various applications, as, for instance, electronic and magnetic devices (2), catalysis (3), nanolasers (4), nanofluidics (5), nanolithography (6) drug delivery, tissue engineering (7), biosensors (8–10), and medicine (11). A very interesting aspect of these nanomaterials is that their physical and chemical properties are tunable via the control of their size and shape (12). Therefore, a formidable challenge is to achieve control over the average size and size distribution of the nanomaterials.

The classic approach to size control that has been used, for example for semiconducting quantum dots, is nucleation and growth (13). An alternative strategy consists of using a template of a precise shape and size to produce nanostructures. For example, on some porous membranes that contain cylindrical pores of uniform diameter, monodisperse nanocylinders of the desired material, whose dimensions can be carefully controlled, can be obtained (14).

For this templating strategy, one promising approach is to use bio-inspired tactics (12, 15) to build the templates. Indeed, within living organisms, efficient strategies can be found to accomplish fully functional and controlled nano-architectures based on the very specific self-assembly of proteins, lipids, and/or DNA in water and in very mild conditions of temperature, pressure, and pH, such as intracellular cytoskeletons, actin filaments, and extracellular collagen assemblies, chromatin, membranes, etc. Moreover, there are numerous examples of composite materials for which the organic part serves as a template for mineralization (16–19). In the field of nanotechnology, the most famous example is the capsid of tobacco mosaic virus, which can be reconstituted in vitro (20) and used as a template for the synthesis and assembly of semiconductor and magnetic nanowires (19, 21). This historical first example has been followed by simpler systems consisting of organic templates formed by small peptides (12, 22, 23).

Therefore, self-assembling properties of synthetic biomimetic molecules have been extensively studied for the same purpose. For example, synthetic lipids such as amphiphilic molecules that append sugar, peptide, and nucleic acid moieties as hydrophilic headgroups (24) form hollow cylindrical architectures that can be further used to incorporate metal particles. Also, since the discovery of amyloid-related diseases, scientists have realized that proteins, but also small peptides, have the general property of forming fibers/nanotubes through a self-assembly process

Author contributions: S.R., F.G., N.F., E.P., M.L., B.R., F.A., M. Paternostre, and J.-C.C. designed research; C.T., S.R., F.G., N.F., E.P., C.M., M.L., D.T., M.I., J.M.V., M. Petitjean, L.P., B.R., F.A., M. Paternostre, and J.-C.C. performed research; S.R., M.L., M.I., F.B., D.B., B.R., F.A., M. Paternostre, and J.-C.C. contributed new reagents/analytic tools; C.T., F.G., N.F., E.P., C.V., B.R., F.A., M. Paternostre, and J.-C.C. analyzed data; and F.G., C.V., B.R., F.A., M. Paternostre, and J.-C.C. wrote the paper.

The authors declare no conflict of interest.

This article is a PNAS Direct Submission.

[1]C.T., S.R., F.G., and N.F. contributed equally to this work

[2]To whom correspondence may be addressed. E-mail: franck.artzner@univ-rennes1.fr, maite.paternostre@cea.fr, or jean-christophe.cintrat@cea.fr.

This article contains supporting information online at www.pnas.org/lookup/suppl/doi:10.1073/pnas.1017343108/-/DCSupplemental.

(25, 26). Therefore, small peptides based on protein sequences have been widely studied for their ability to form well-defined nano-architectures, in particular those forming β-sheet stabilized nanotubes and fibers (27) or fibrous materials from α-helical peptides (28, 29). The first examples of synthetic peptide nanotubes were obtained by Ghadiri and coworkers (30) in a small diameter range—i.e., from 0.7 to 1.3 nm. These hollow tubes are formed by the one-dimensional packing of alternating D- and L-amino acid cyclic peptides through an antiparallel β-sheet network. Later, other libraries of small diameter nanotubes (internal diameter smaller than 2.4 nm) have been synthesized from either amphiphilic dendritic dipeptides (31) or hydrophobic dipeptides (32). There are also a few examples of nanotubes with large either polydisperse or monodisperse diameters obtained with surfactant-like peptides (33), lipid-peptides as the bola-amphiphiles developed by Matsui and coworkers (34), or amyloid peptides at acidic pH (35).

However, despite the numerous systems studied, there are few examples of strictly monodisperse nanotubes formed by biomimetic molecules (36). In an attempt to control the size of self-assemblies built from biomimetic molecules, Shimizu's group developed "wedge-shaped" amphiphiles, in which two hydrophilic moieties of different size are covalently linked to the two ends of a hydrophobic spacer (37). They theoretically proposed by using a simple geometrical model and experimentally showed that they can control the inner diameter of multilayered nanotubes by varying the length of the hydrophobic spacer (38).

Until now, none of these studies allowed production of a library of nanotubes covering a wide range of controlled and monodisperse diameters. In all these examples, the self-assemblies are achieved by rather simple molecular packing: either one-dimensional packing of cyclic peptides or one- and two-dimensional packing of amphiphilic peptides and/or lipids forming nanotubes, fibers, or lamellae. In the field of synthetic biomimetic molecule self-assembly, the 24-nm-wide nanotubes formed by Lanreotide exhibit as many as four different hierarchical levels of order within the structure and show an unprecedented level of monodispersity. This simple system is, in the field of peptide self-assembly, one of the most carefully characterized in terms of structure (36, 39) and mechanisms of formation (40). Moreover, its self-assembly properties are already used in medicine with Autogel®, a sustained release formulation formed by a high concentration of peptide in water. Finally, we have also shown that these nanotubes can be used as template for mineralization (41). Therefore, if the capacity of Lanreotide for forming nanotubes perfectly calibrated in diameter and the possibility of mineralizing these nanotubes are already interesting features for nanotechnology, Lanreotide is also an attractive system because it can be studied as a model allowing fundamental insight into self-assembly mechanisms that should increase our understanding and therefore our control of these phenomena. The aim of the present work is to find the molecular keys allowing the diameter control of the nanotubes.

One of the most noteworthy features of Lanreotide nanotubes is that their walls are curved two-dimensional crystals, and this high degree of order led us to work on a structural approach. Indeed, the structure of the nanotube walls and further evidence from studies on derivatives (42, 43) suggested that the amino acids involved in close contact between peptides could play a role in setting the nanotube diameter. Moreover, the recently elucidated mechanism of formation of these nanotubes shows that the curvature radius of the nanotube is fixed at a very early stage of the assembly—i.e., before the nanotube closure, upholding the idea that molecular determinants control the curvature radius of the final nanotubes (40). We therefore based the present work on a central hypothesis—i.e., the size of the amino acids involved in the close contact between peptides within the crystalline walls of the nanotubes directly control the diameter of the nanotubes. All the strategy of this work is based on the size modification of one precise aromatic amino acid, and we demonstrate that this approach does indeed enable the accurate tuning of the diameter of the nanotubes from 9 to 35 nm while keeping their monodispersity.

Results

Peptide Design. Lanreotide (NH-D-2-Nal-cyclo-[Cys-Tyr-D-Trp-Lys-Val-Cys]-Thr-$CONH_2$) is an octapeptide cyclized by a disulfide bridge (Fig. 1). Its sequence has some very peculiar features, such as (*i*) three of the eight amino acids are aromatics, (*ii*) the peptide is positively charged in pure water (at the N terminus and on the Lys), (*iii*) two of the amino acids are in the D conformation, and (*iv*) one of the aromatic residues is unnatural (D-2-Nal) (Fig. 1*A*).

Lanreotide self-assembles reversibly into micrometer-long, hollow nanotubes with a rigorously monodisperse diameter (24.4 nm) (36). The low-resolution structure of the nanotube wall shows that the peptides are stacked in a two-dimensional curved crystal in which lanreotide is packed in a two-dimensional monoclinic lattice with $i = 20.7$ Å, $j = 20.8$ Å, $\gamma = 117.2°$. The j vector that is at an angle of 48.3° with respect to the direction of the cylinder axis follows the direction of the antiparallel H-bound network, and the i vector at an angle of 68.9° is due to lateral packing of the peptides through aromatic interactions. The wall thickness of 18 Å implies that the building block of the nanotubes is a dimer. Moreover, due to a systematic segregation of the aromatic moiety of the molecule, it is a face-to-face dimer.

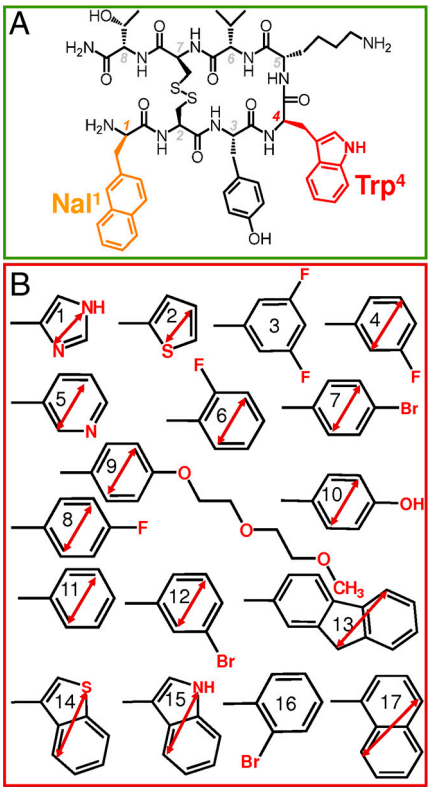

Fig. 1. Structure of lanreotide (*A*) and of the 17 derivatives (*B*). The numbers on the aromatic moieties identify the 17 derivatives as follows: 1, [D-Histidine]^4; 2, [β-2-thienyl-D-Alanine]^4; 3, [3,5-Difluoro-D-Phenylalanine]^4; 4, [m-Fluoro-D-phenylalanine]^4; 5, [β-(3-pyridyl)-D-Alanine]^4; 6, [o-Fluoro-D-Phenylalanine]^4; 7, [p-Bromo-D-Phenylalanine]^4; 8, [p-Fluoro-D-Phenylalanine]^4; 9, [2-(2-methoxyethoxy)-ethoxy-D-Tyrosine]^4 or ([D-Tyrosine-DEG]^4); 10, [D-Tyrosine]^4; 11, [D-Phenylalanine]^4; 12, [m-Bromo-D-Phenylalanine]^4; 13, [β-(2-fluorenyl)-D-Alanine]^4; 14, [β-(3-benzothienyl)-D-Alanine]^4; 15, Lanreotide; 16, [o-Bromo-D-Phenylalanine]^4; 17, [β-(1-naphthyl)-D-Alanine]^4. The red arrows on each molecule represent the molecular size parameter that correlates with the geometrical model (see text for details). Two molecules (the third and the 16th) did not correlate with the model.

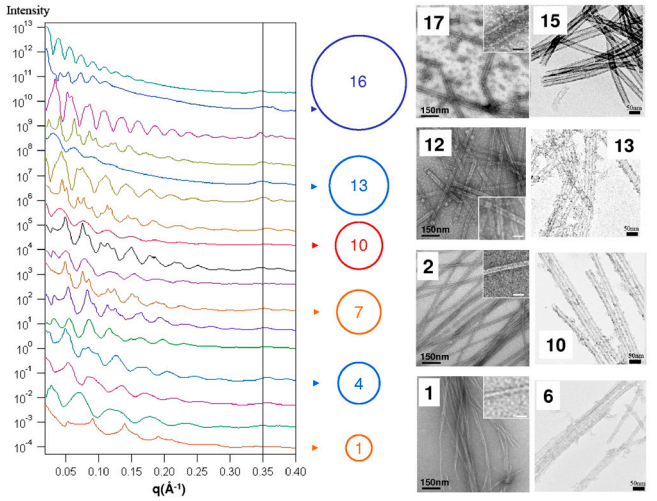

Fig. 2. SAXS (*Left*) and electron micrographs (*Right*) of peptide nanotubes (left column of *Right*) and mineralized peptide nanotubes (right column of *Right*). (*Middle*) Illustration of the evolution of the nanotube size (the numbers refer to the derivative numbers illustrated in Fig. 1). (*Left*) The SAXS patterns are plotted from the bottom to the top for all 17 derivatives. The diffraction peaks are not resolved, but their envelope (form factor) is observed. Except for peptides 8, 10, and 13, all the SAXS patterns exhibit the Bragg peaks that originate from the packing of the nanotube in a hexagonal lattice. (*Right*) Electron micrographs of nanotubes negatively stained by uranyl acetate peptide–water solutions at 5% (w/w) (left column) and peptide nanotubes coated with silica (right column). The numbers on each micrograph refer to the derivative number. Scale bar: 150 nm. (*Inset*) (left column) Zoom on the nanotubes. Scale bar: 50 nm.

The structures of the two peptide layers (Fig. 3 *A* and *B*) are different in terms of molecular packing and close contacts. Aromatic lateral chains are particularly important for the cohesion of peptide self-assemblies (44) because their stacking driven by hydrophobic effect is geometrically controlled by the rigidity of the aromatics itself. Therefore it was very interesting to note that within the walls of Lanreotide nanotubes, the two aromatics D-Nal and D-Trp are involved in the close contacts within the crystal but each on a different layer (Fig. 3 *A*, *A*/*B*, and *C*). Previous results showed that the mutation of D-Trp into D-Phe led to the formation of monodisperse nanotubes of 18-nm width instead of 24 nm, while keeping an identical molecular and supramolecular organization (36, 43). The hypothesis tested in this study is that the close contacts drive the curvature radius of the crystal and therefore the nanotube diameter. Therefore, the Trp in position 4 was replaced by 16 different aromatic side chains whose structures are shown in Fig. 1. To demonstrate the generality of this approach we chose to incorporate aromatic structures consisting of mono- (derivatives 1 to 12 and 16), di- (derivatives 14, 15, and 17), and tri-cycles (derivative 13). These cycles could either incorporate one (derivatives 2, 5, 14, and 15) or two heteroatoms (derivative 1) such as sulfur or nitrogen or bear a substitution such as fluorine (derivatives 3, 4, 6, and 8), bromine (derivatives 7, 12, and 16), or oxygen (derivative 9).

Nanotube Characteristics. Compounds 1 to 17 spontaneously self-assemble in aqueous solution into nanotubes as shown by small angle X-ray scattering (SAXS) and electron microscopy (Fig. 2). If the electron micrographs show different diameters depending on the peptide sequence they are unsuitable for size determination, because the procedure itself induces some deformation of the nanotube in particular due to the drying of the sample on the grid. Therefore, the precise diameters of the nanotubes were extracted from the SAXS patterns. The X-ray patterns recorded for the 17 peptides are superimposed in Fig. 2 *Left*. All the patterns exhibit regular oscillations that can be attributed univocally to the form factor of monodisperse hollow cylinders. These regular oscillations are well fitted by normalized Bessel functions of zero order $[J_0(q \cdot r_0)/q \cdot r_0]^2$. This mathematical model is the theoretical form factor of infinite hollow columns (45), where the only variable parameter is the mean radius of the column r_0. The high number of Bessel oscillations (up to 12) demonstrates the monodispersity of the nanotube radii within a given sample (see Fig. S1). The increase of polydispersity within the sample rapidly induces the decrease of the number of the oscillation on the X-ray pattern (see Fig. S1) and is therefore the approach we used to determine the polydispersity index of our sample. In our case, for all the nanotubes except 2 (those formed with derivative 13 ([β-(2-fluorenyl)-D-Alanine]) and 16 ([o-Bromo-D-Phenylalanine][4]), the polydispersity is lower than 3%. For derivatives 13 and 16, the polydispersity is about 5%. Aside from this very good polydispersity index for all the samples, these results demonstrate unambiguously that the radii of the nanotubes depend on the peptide sequence and in particular on the structure and size of the side chain in the fourth position. The correlation of the minima between adjacent oscillations with the zero of the Bessel function gives access to the diameter of the nanotubes as reported in Fig. 2 and Table 1.

Another argument in favor to the monodispersity of the nanotubes is that Bragg peaks are visible on the majority of the SAXS patterns (13 patterns over 17), indicating a crystallization that can occur only with monodisperse nanotubes. These reflections can be indexed by a hexagonal lattice model that reveals the crystallization of the nanotubes in a hexagonal network. Interestingly, the hexagonal parameter depends on the nanotube diameter. In our previous work (36, 43) we proposed that, due to electrostatic repulsion, a separate nanotube cannot exist but is stabilized by the vicinity of other ones, explaining the organization of the lanreotide nanotube in a hexagonal lattice. Moreover, by a simple calculation, we proposed that, to be at equilibrium, the distance between the nanotubes should be about the nanotube radius, leading to a hexagonal parameter of approximately $3R$ (36). For all the 13 derivatives exhibiting Bragg peaks, we found that the average ratio between the hexagonal parameter and the diameter is about 2.9 ± 0.4, confirming the previous hypothesis (see Table 1).

Finally, all the SAXS patterns recorded for the derivatives exhibit the same three reflections between 0.35 $Å^{-1}$ and 0.37 $Å^{-1}$ (gray line in Fig. 3). For lanreotide, it was previously shown that these reflections, corresponding to repetitive distances between 17 $Å^{-1}$ and 18 $Å^{-1}$, arise from an antiparallel β-sheet network (36) built between the molecules to form the wall of the nanotubes. The signature of the β-sheet network indicates that the lanreotide-type molecular packing is preserved in these new peptide nanotubes.

Nanotube Mineralization. These nanotubes of different diameters can be used as templates for mineralization with silica, as already obtained for lanreotide nanotubes (41) (Fig. 2, electron micrographs on the right panel; and Table 1). The electron micrographs demonstrate the mineralization of the nanotubes as no staining was used, the electron density of silica being high enough for a direct visualization. Moreover, the diameters of the composite nanotubes, measured from TEM micrographs are in good agreement with the pure peptide nanotubes (Table 1), indicating that the peptide organization is not altered by the interaction with silica. Moreover, composite nanotubes of increasing size from 13 to 29 nm have been synthesized, demonstrating the potential use of these nanotubes of controlled sizes as templates for mineralization.

Geometrical Model. The nanotube wall is formed by a peptide bilayer that protects the hydrophobic aliphatic and aromatic residues from water (Fig. 3 *A*/*B*, red and blue, respectively) and exposes the hydrophilic one to water (Fig. 3*A*/*B*, green). The

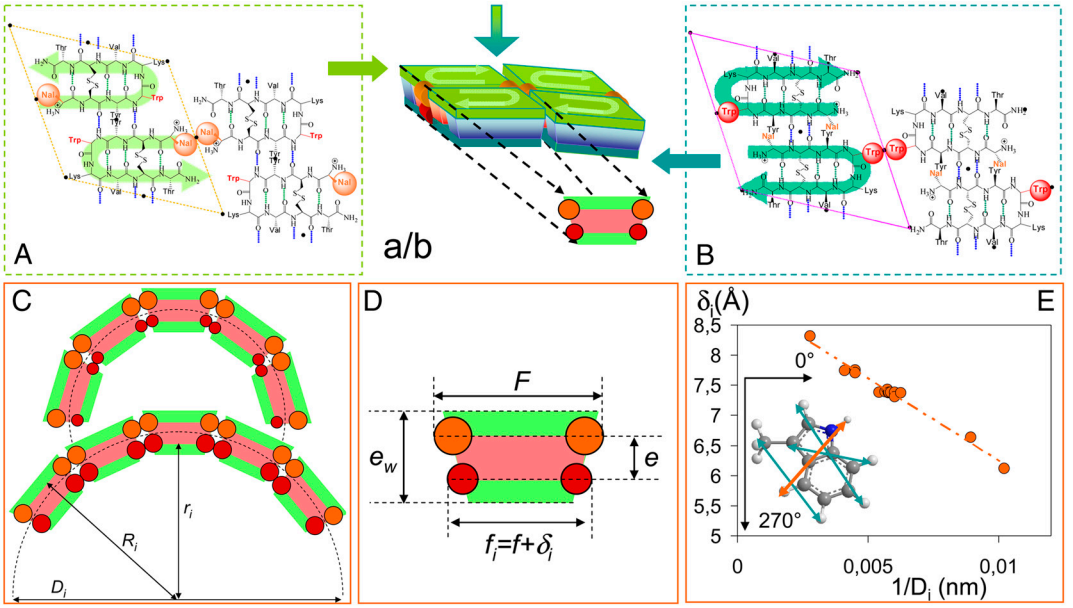

Fig. 3. Geometrical model and correlation between the size of the aromatic residue of the derivatives and the nanotube diameter. (*A*, *A/B*, and *B*) The nanotube wall (*A/B*) is formed by the stacking of the two different layers shown on *A* and *B*. These two layers are not equivalent: The intermolecular H bonds of the filament involve different residues as well as the lateral packing of the filaments. In particular, the close contact between the filaments in the external layer involves the aromatic Nal residue (*A*, underlined in orange), whereas it involves the Trp in the internal layer (*B*, underlined in red). These two layers superimposed with the C2 axes (black dots) form a bilayer (*A/B*) that exposes the hydrophilic residues to water (green surfaces) and protects the hydrophobic aromatic (red) and the hydrophobic aliphatic (blue) residues from water. The red and orange circles show the internal and external contact, respectively—i.e., the Trp and Nal residues. The unit cell of the bilayer is shown in the lower part of *A/B* as a trapezium. The green and red underline the hydrophilic nature of the surfaces of the walls and the aromatic core of the bilayer, respectively. The external Nal and internal Trp close contacts are shown as orange and red circles. (*C*) Illustration of the influence of the size of the internal Trp close contact on the nanotube diameter and definition of the geometrical parameters D_i, R_i, and r_i. (*D*) Definition of the geometrical parameters of the repetitive structural unit shown in *A/B*: e_w, e, *F*, f_i *f*, and δ_i. δ_i represents the size parameter of the aromatic residue in position 4 of the peptide sequence. (*E*) Relationship between aromatic size and nanotube diameter. The straight line comes from the model and the orange points are from the experiments. This figure shows the best fit between experiment and theory considering that different aromatic sizes have been tested as shown for Trp in the inset. The best fit gave 0.69 nm for e and 1.07 for f, close to the experimental values (see text for details).

internal (Fig. 3*A*) and external layers (Fig. 3*B*) are formed by the lateral packing of amyloid-like filaments—i.e., peptides linked by an intermolecular antiparallel β-sheet network. As shown in Fig. 3 *A* and *B*), the two layers are not equivalent because the intermolecular H-bond network and the close contacts between the filaments involve different amino acids. Indeed, on one layer, the close contact between the filaments involves the D-Trp (Fig. 3*B*, underlined in red) and on the other the D-Nal (Fig. 3*B*, underlined in orange). Considering the importance of aromatic lateral chains in peptide self-assemblies (44, 46), the fact that these two aromatic lateral chains could act as lever arms in the structure appears very attracting.

In previous experiments, we showed that changing the D-Nal of the lanreotide sequence into a D-Phe abolished the self-assembly properties, whereas the analogue where the D-Trp was replaced by a D-Phe kept similar self-assembly properties (36).

Table 1. Comparison between experimental and theoretical structural parameters of the nanotubes

#	Derivative name	Hexagonal parameter (Å)	Diameters (+/ − 4 Å) (polydispersity index)	δ_i (Å)	Theoretical diameters (Å)	Difference%	Diameters silicated nanotubes (Å)
1	[D-Histidine][4]	140	98 (<3%)	6.121	96	2	n.d.
2	[D-Thienyl][4]	165	112 (<3%)	6.633	117	5	n.d.
3	[3,5-Difluoro-D-Phenylalanine][4]	235	148 (<3%)	7.874	248	69	n.d.
4	[m-Fluoro-D-phenylalanine][4]	255	160 (<3%)	7.373	171	7	n.d.
5	[β-(3-pyridyl)-D-Alanine][4]	228	166 (<3%)	7.308	164	1	n.d.
6	[o-Fluoro-D-Phenylalanine][4]	230	166 (<3%)	7.379	171	3	154 ± 12
7	[p-Bromo-D-Phenylalanine][4]	255	170 (<3%)	7.386	172	1	n.d.
8	[p-Fluoro-D-Phenylalanine][4]	-	172 (<3%)	7.379	171	<1	129 ± 3
9	[D-Tyrosine-DEG][4]	248	173 (<3%)	7.371	170	1	n.d.
10	[D-Tyrosine][4]	-	174 (<3%)	7.426	176	1	n.d.
11	[D-Phenylalanine][4]	280	177 (<3%)	7.388	172	6	205 ± 15
12	[m-Bromo-D-Phenylalanine][4]	287	184 (<3%)	7.386	172	1	n.d.
13	[β-(2-fluorenyl)-D-Alanine][4]	-	222 (5%)	7.707	216	3	220 ± 20
14	[β-(3-benzothienyl)-*D*-Alanine][4]	309	222 (<3%)	7.754	224	1	n.d.
15	Lanreotide	364	244 (<3%)	7.745	222	9	290 ± 30
16	[o-Bromo-D-Phenylalanine][4]	350	288 (5%)	7.370	170	41	n.d.
17	[β-(1-naphthyl)-D-Alanine][4]		360,5 (<3%)	8.316	417	15 4 (average)	n.d.

Experimental structural parameters (hexagonal lattice, nanotube diameters, and polydispersity index determined from SAXS patterns); size hindrance parameter δ_i measured with Chem3DUltra; theoretical diameters calculated from the geometrical model; difference between experimental and theoretical diameters in % and diameters of the mineralized nanotubes.

Moreover, the nanotubes spontaneously formed were monodisperse in diameter but smaller than those obtained with lanreotide. In this study we therefore focused on the D-Trp substitution and synthesized 16 different peptides.

We first confirm that the layer involving the Trp in close contact between adjacent filaments (Fig. 3*B*) is in fact the internal layer of the nanotube. In a first analysis, the size increase of the aromatic side chain in position 4 induces an increase in the diameter. If the close contact generated by the Trp had been on the external layer, the size increase would have induced a decrease in the nanotube diameter as shown in Fig. 3*C*.

From this simple consideration we built a geometrical model based on the simplified projection of the unit cell (Fig. 3 *A*/*B* and *D*). This model shows a perpendicular cut of the bilayer, the red layer sandwiched in between two green ones corresponds to the aromatic interior of the bilayer, and the orange and red circles represent the D-Nal and D-Trp supporting the close contacts in the external and internal layer, respectively. In this model e is the distance between the external and internal close contacts ($e = e_w/2$, e_w being the wall thickness), and F and f_i are the lengths between two close contacts on the external and internal layer, respectively—i.e., between two D-Nal for the external layer and between two D-Trp on the internal layer. In this model F is constant and f_i can be expressed by a constant length f and δ_i, which is the characteristic length of the aromatic in the fourth position. From this model, we determined the relationship between δ_i and the nanotube diameter D_i (Fig. 3*C*), $\delta_i = F\text{-}f\text{-}(2F\frac{e}{Di})$ (see *SI Text* for details). This relationship (only valid for e/D_i close to zero) shows a linear dependence of δ_i on the inverse of D_i, the slope being equal to $(F\text{-}f)$ and the origin to $(-2Fe)$.

To test this model, we looked for the relevant distance of the aromatic moiety. First of all, the fact that these lateral chains are built from aromatics also means that these chemical groups are rigid, making the distance measurement easy. Nevertheless, the difficulty comes from the fact that the structure determined for Lanreotide nanotubes is not an atomic one, and, consequently, there is no precise indication of the orientation of the aromatic moiety within the nanotube wall. In solution, the aromatics are free to rotate, and in the nanotube wall they probably adopt a fixed conformation adapted to the molecular packing. Therefore, to verify this geometrical model, we should test all possible distances δ_i. These distances have been measured and classified into different sets depending on the angle between the C_{ala}-C_{ϕ} bond and the distance measured (see *SI Text* for details). For each set of distance we plot δ_i versus $1/D_i$ and fit the best straight line, leaving the origin and the slope as adjustment parameters. The results of these fits were then examined, and only four fits giving reasonable values for e and f were kept (see Table S1 for details). To discriminate between these four different fits, the structural parameters e and f were determined from the slope and the origin of the fitted straight lines after fixing F to 19.7 Å, in agreement with the unit cell parameters (36). In Fig. 3*E* the best fit and the distance measurements schematized on Trp are superimposed together (see SI Text for the other fits). The red arrow indicates the one that fits the geometrical model (the size parameter fitting with the model is indicated for each residue by a red arrow in Fig. 1). The values for e and f extracted from the fit are 6.9 Å and 10.7 Å, respectively, in very good agreement with the structural data (36). Table 1 shows the experimental and calculated values of the nanotube diameters. Except for two of the 17 derivatives (3 and 16), the agreement with the experimental and theoretical diameter is very good; i.e., the average difference between the experimental and the theoretical values is below 4%. This model also predicts the maximal size of the aromatic, as for $F = f$ the curvature radius will be infinite; i.e., this limit would be reached for a characteristic size of the aromatic $\delta_i = 10.7$ Å.

Discussion and Conclusions

In the literature, attempts to control the size of nano-architectures by chemical structure modification have very often failed. Indeed, whereas monodispersity can be achieved, there have been very few examples of successful size tuning by chemical modification. One example is the modulation of the inner diameter of polydisperse multilayer lipid nanotubes formed by a bola-amphiphile. The number of layers could not be controlled, but the inner diameters of the self-assembled nanotubes could be increased from 15 to 22 nm at intervals of 1.5 nm on average by lengthening the oligomethylene spacer by two carbon atoms (38). In our case, the wall of the nanotubes is 2D curved crystal of peptides leading to perfectly monodisperse diameters between 10 and 36 nm. The reason for this success comes from the in-depth knowledge we previously acquired on the structure of the lanreotide nanotubes as it allowed the identification of one of the lever arm that directly influence the diameter of the nanotube. Therefore, this study underlines that, in the perspective of using self-assembly phenomena in nanotechnology, the precise characterization not only of the architecture morphology but also of their molecular and supramolecular structure is a prerequisite to monitor the size and shape of the self-assembled architecture.

Uniquely, the diameter of nanotubes has been precisely tuned over such a wide range by chemical modification of the building blocks without changing monodispersity and keeping the fascinating organization of lanreotide. Moreover, these diameters can be predicted with an average accuracy of about 4% by a simple geometrical model that explains how a size increase of about 2 Å on a side chain of a peptide sequence induces a diameter increase from 10 to 36 nm. We also show that these new monodisperse peptide nanotubes can be used as templates for biomineralization, because double-walled silica nanotubes with monodisperse diameters self-organized into highly ordered centimeter-sized fibers were synthesized. This fine control of the diameter of silica nanotubes opens the way to a wide range of applications in nanotechnology, such as optical fibers, nano-filtration, and chemical reservoirs.

Material and Methods

Chemicals. Amino acid derivatives were from Bachem, Fluka, Acros Organics, and NeoMPS. Peptide synthesis resin was from Novabiochem (Merck Bioscience) and ion-exchange resin from Bio-Rad Laboratories Inc. Peptides 11 and 15 were supplied by IPSEN Pharma.

Deionized water (18 MΩ) was obtained using a Millipore Milli-Q Plus resin exchanger. Scavengers, coupling agents, cleavage reagents, and solvents for synthesis and RP-HPLC were from Aldrich and VWR products and were used without further purification.

Peptide Synthesis and Purification. Synthesis of cyclic peptides was performed by Fmoc/tBu solid phase peptide synthetic method. The peptide chain was first assembled and then cyclized on-resin. Cleavage and side chain deprotection were performed simultaneously, followed by purification and counter ion exchange (47). Purity of the final products was checked by HPLC/MS (see *SI Text* for details on amino acids and peptide synthesis).

LC/MS Analysis and Purification. HPLC was performed using a Waters system (2525 binary gradient module, in-line degasser, 2767 sample manager, 2996 Photodiode Array Detector). The eluent was a gradient of A (99.9% water / 0.1% HCOOH) and B (99.9% ACN / 0.1% HCOOH). Either analytical or preparative X-bridge C18 columns were used. The mass spectrometer was a Waters Micromass ZQ system with a ZQ2000 quadrupole analyzer. The ionization was performed by electrospray and the other parameters were as follows: source temperature 120 °C, cone voltage 20 V, and continuous sample injection at 0.3 mL/ min flow rate. Mass spectra were recorded in positive ion mode in the m/z 100–2,000 range and treated with the Mass Lynx 4.0 software.

NMR Analysis. ^{1}H-NMR experiments were performed on a Bruker Avance 400 Ultrashield. Spectra were recorded at room temperature at 400 MHz, samples were dissolved in D_2O at a concentration of approximately 5 mM. The D_2O singlet signal was set up at 4.79 ppm. Chemical shifts are given in ppm and the coupling constants in Hz (see *SI Text* for details on the peptide characterization).

Negative Staining. The lanreotide solution was deposited onto freshly glow-discharged 400-mesh collodion/carbon-coated grids and allowed to settle for 1 min. Grids were then quickly blotted, briefly rinsed with distilled water, and stained with uranyl acetate solution (2%). The grids were then observed with a Philips CM12 microscope operating at 80 kV.

Small Angle X-ray Scattering (SAXS). SAXS was performed on the high brilliance SWING beam line (12 KeV) at the Soleil Synchrotron Facility (48) using sample-detector distances of 0.5 to 1 m depending on the experiments. The diffraction patterns were therefore recorded for reciprocal spacing q ($Å^{-1}$) from 0.02 to 2.1 $Å^{-1}$—i.e., a range of repetitive distances $d = 2\pi/q$ from 310 Å and 3 Å. The X-ray patterns were detected and recorded via a chip charge-coupled device camera detector.

The samples were prepared in 1.3–1.6 mm glass capillaries (Glas Technik and Konstruktion, Schönewalde bei) and introduced into a homemade capillary holder accommodating 20 capillaries at controlled temperature or subject to a computer-monitored controlled temperature program. All samples exhibited powder diffraction and scattering intensities as a function of the radial wave vector, $q = 4\pi \sin\theta/\lambda$, which was determined by circular integration.

Synthesis of the Silicated Nanotubes. The synthesis of silicated nanotubes was realized as described (41) for silicated nanotubes of lanreotide. Peptide nanotube gels were prepared at ambient temperature using peptide acetate powder dissolved in pure water (5% w/w). The silica precursor solution was an emulsion of TEOS in water (30% w/w), prepared 24 h before use. The fiber syntheses were carried out in 1.5 mm glass capillaries (GLAS Technik & Konstruktion). The samples were prepared by sequential deposition of 15 μL of peptide gel and then 15 μL of the silica precursor in the capillary. The fibers appeared after a time ranging from 48 h to one week. The resulting white fibers were removed from the tube and dried under vacuum at 80 °C.

ACKNOWLEDGMENTS. This work was supported by the biotechnology program of the French Agency for Research (ANR) with the Thera-Pep project. S.R. and F.G. were paid by Commissariat à l'Énergie Atomique et aux Énergies Alternatives, which we greatly acknowledge. The Région Bretagne is acknowledged for the PhD fellowship of C.T. Synchrotron SOLEIL (France) is acknowledged for beam time allocation (proposal 20100148), and Florian Meneau in particular for his assistance during the synchrotron runs.

1. Bawendi MG, Steigerwald ML, Brus LE (1990) The quantum mechanics of larger semiconductor clusters (quantum dots). *Annu Rev Phys Chem* 41:477–496.
2. Lu W, Lieber CM (2006) Semiconductor nanowires. *J Physics D Appl Phys* R387–R406.
3. Bell AT (2003) The impact of nanoscience on heterogeneous catalysis. *Science* 299:1688–1691.
4. Pauzauskie PJ, Yang P (2006) Nanowire photonics. *Mater Today* 9(10):36–45.
5. Sopher NB, Abrams ZR, Reches M, Gazit E, Hanein Y (2007) Integrating peptide nanotubes in micro-fabrication processes. *J Micromech Microeng* 17:2360–2365.
6. Kim DS, et al. (2007) Laser-interference lithography tailored for highly symmetrically arranged ZnO nanowire arrays. *Small* 3:76–80.
7. Zhang S (2008) Designer self-assembling peptide nanofiber scaffolds for study of 3-D cell biology and beyond. *Adv Cancer Res* 99:335–362.
8. Patolsky F, Zheng GF, Lieber CM (2006) Nanowire-based biosensors. *Anal Chem* 78 (13):4260–4269.
9. Werner S, Marillonnet S, Hause G, Klimyuk V, Gleba Y (2006) Immunoabsorbent nanoparticles based on a tobamovirus displaying protein A. *Proc Natl Acad Sci USA* 103:17678–17683.
10. Willner I, Baron R, Willner B (2007) Integrated nanoparticle-biomolecule systems for biosensing and bioelectronics. *Biosens Bioelectron* 22:1841–1852.
11. Moghimi SM, Hunter AC, Murray JC (2005) Nanomedicine: Current status and future prospects. *FASEB J* 19:311–330.
12. Gao XY, Matsui H (2005) Peptide-based nanotubes and their applications in bionanotechnology. *Adv Mater* 17:2037–2050.
13. Murray CB, Norris DJ, Bawendi MG (1993) Synthesis and characterization of nearly monodisperse Cde ($E = S$, Se, Te) semiconductor nanocrystallites. *J Am Chem Soc* 115:8706–8715.
14. Martin CR (1996) Membrane-based synthesis of nanomaterials. *Chem Mater* 8:1739–1746.
15. Portney NG, et al. (2007) Microscale memory characteristics of virus-quantum dot hybrids. *Appl Phys Lett* 90:214104.
16. Olszta MJ, et al. (2007) Bone structure and formation: A new perspective. *Mater Sci Eng R Rep* 58:77–116.
17. Mann S, et al. (1997) Sol-gel synthesis of organized matter. *Chem Mater* 9:2300–2310.
18. Estroff LA, Hamilton AD (2001) At the interface of organic and inorganic chemistry: Bioinspired synthesis of composite materials. *Chem Mater* 13:3227–3235.
19. Dujardin E, Peet C, Stubbs G, Culver JN, Mann S (2003) Organization of metallic nanoparticles using tobacco mosaic virus templates. *Nano Lett* 3:413–417.
20. Fraenkel-Conrat H, Williams RC (1955) Reconstitution of active Tobacco Mosaic virus from its inactive protein and nucleic acid components. *Proc Natl Acad Sci USA* 41:690–698.
21. Shenton W, Douglas T, Young M, Stubbs G, Mann S (1999) Inorganic-organic nanotube composites from template mineralization of tobacco mosaic virus. *Adv Mater* 11:253–256.
22. Reches M, Gazit E (2003) Casting metal nanowires within discrete self-assembled peptide nanotubes. *Science* 300:625–627.
23. Koopmans RJ, Aggeli A (2010) Nanobiotechnology—quo vadis? *Curr Opin Microbiol* 13:327–334.
24. Shimizu T (2008) Molecular self-assembly into one-dimensional nanotube architectures and exploitation of their functions. *Bull Chem Soc Jpn* 81:1554–1566.
25. Mehta AK, et al. (2008) Facial symmetry in protein self-assembly. *J Am Chem Soc* 130:9829–9835.
26. Dobson CM (2003) Protein folding and misfolding. *Nature* 426:884–890.
27. Hamley IW (2007) Peptide fibrillization. *Angew Chem Int Ed Engl* 46:8128–8147.
28. Woolfson DN, Ryadnov MG (2006) Peptide-based fibrous biomaterials: Some things old, new and borrowed. *Curr Opin Chem Biol* 10:559–567.
29. Ryadnov MG, Woolfson DN (2003) Introducing branches into a self-assembling peptide fiber. *Angew Chem Int Ed Engl* 42:3021–3023.
30. Ghadiri MR, Granja JR, Milligan RA, McRee DE, Khazanovich N (1993) Self-assembling organic nanotubes based on a cyclic peptide architecture. *Nature* 366:324–327.
31. Percec V, et al. (2004) Self-assembly of amphiphilic dendritic dipeptides into helical pores. *Nature* 430:764–768.
32. Görbitz CH (2001) Nanotube formation by hydrophobic dipeptides. *Chem-Eur J* 7:5153–5159.
33. Vauthey S, Santoso S, Gong H, Watson N, Zhang S (2002) Molecular self-assembly of surfactant-like peptides to form nanotubes and nanovesicles. *Proc Natl Acad Sci USA* 99:5355–5360.
34. Matsui H, Gologan B (2000) Crystalline glycylglycine bolaamphiphile tubules and their pH-sensitive structural transformation. *J Phys Chem B* 104:3383–3386.
35. Lu K, Jacob J, Thiyagarajan P, Conticello VP, Lynn DG (2003) Exploiting amyloid fibril lamination for nanotube self-assembly. *J Am Chem Soc* 125:6391–6393.
36. Valery C, et al. (2003) Biomimetic organization: Octapeptide self-assembly into nanotubes of viral capsid-like dimension. *Proc Natl Acad Sci USA* 100:10258–10262.
37. Masuda M, Shimizu T (2001) Multilayer structure of an unsymmetrical monolayer lipid membrane with a 'head-to-tail' interface. *Chem Commun* 23:2442–2443.
38. Masuda M, Shimizu T (2004) Lipid nanotubes and microtubes: Experimental evidence for unsymmetrical monolayer membrane formation from unsymmetrical bolaamphiphiles. *Langmuir* 20:5969–5977.
39. Valery C, et al. (2004) Self-association process of a peptide in solution: from beta-sheet filaments to large embedded nanotubes. *Biophys J* 86:2484–2501.
40. Pouget E, et al. (2010) Elucidation of the self-assembly pathway of lanreotide octapeptide into beta-sheet nanotubes: Role of two stable intermediates. *J Am Chem Soc* 132:4230–4241.
41. Pouget E, et al. (2007) Hierarchical architectures by synergy between dynamical template self-assembly and biomineralization. *Nat Mater* 6:434–439.
42. Pandit A, et al. (2008) Self-assembly of the octapeptide lanreotide and lanreotide-based derivatives: The role of the aromatic residues. *J Pept Sci* 14:66–75.
43. Valery C, et al. (2008) Molecular origin of the self-assembly of lanreotide into nanotubes: a mutational approach. *Biophys J* 94:1782–1795.
44. Reches M, Porat Y, Gazit E (2002) Amyloid fibril formation by pentapeptide and tetrapeptide fragments of human calcitonin. *J Biol Chem* 277:35475–35480.
45. Oster G, Riley DP (1952) Scattering from cylindrically symmetric systems. *Acta Crystallogr* 5:272–276.
46. Gazit E (2007) Self-assembled peptide nanostructures: The design of molecular building blocks and their technological utilization. *Chem Soc Rev* 36:1263–1269.
47. Roux S, et al. (2008) Elimination and exchange of trifluoroacetate counter-ion from cationic peptides: a critical evaluation of different approaches. *J Pept Sci* 14:354–359.
48. David G, Perez J (2009) Combined sampler robot and high-performance liquid chromatography: A fully automated system for biological small-angle X-ray scattering experiments at the Synchrotron SOLEIL SWING beamline. *J Appl Crystallogr* 42:892–900.